INFLUENCE OF THE DIFFUSER VANE SETTING ANGLE ON THE FLOW FIELD IN A RADIAL PUMP

A. Boccazzi[1] *– R. Sala*[2] *– P. Gaetani*[3]

[1)] CNR – IENI, Milano, Italy, aldo.boccazzi@polimi.it
[2)] Università di Pavia, Facoltà di Ingegneria, Pavia, Italy, rsala@unipv.it
[3)] Politecnico di Milano, Dipartimento di Energia, Milano, Italy, paolo.gaetani@polimi.it

ABSTRACT

Particle image velocimetry (2D-PIV) has been used for the investigation of the time averaged flow field inside the vaned diffuser of a centrifugal pump operating at best efficiency point. Pump performances and the diffuser flow field were analysed for three different vane setting angles. It was evidenced that the best efficiency point flow coefficient decreases with the diffuser setting angle reduction. A boundary layer thickness growth on the pressure side, which increases as the flow coefficient decreases, was also shown. No evident separation was ever seen on the diffuser vane suction side even with a sharp diffuser vane LE, used in a previous investigation. The total pressure loss coefficient, obtained from the classical expression proposed by Lieblein for linear cascades, was found to decrease as the setting angle increases. It was evidenced an influence of the diffuser vane setting angle on the impeller slip and an over-turning of the diffuser flow field, at mid-span, with an under-turning at the hub and the shroud, suggesting the occurrence of significant secondary flows.

NOMENCLATURE

BEP best efficiency point
c vane chord
D diameter
K total pressure loss coefficient (eq. 8)
LE vane leading edge
PS vane pressure side
s percentage of diffuser span (s = 0, at hub)
SS vane suction side
TE vane trailing edge
u measured horizontal velocity component
$\vec{U}_2$ peripheral velocity at impeller discharge
v measured vertical velocity component
$\vec{v}$ measured velocity vector
$\vec{v}^*$ non dimensional velocity vector: $\vec{v}^*/\vec{U}_2$
v_r radial velocity component
x horizontal coordinate of PIV mesh
y vertical coordinate of PIV mesh
α absolute flow angle (from tang. direction)
α^* diffuser vane LE mean line angle (setting angle, from tang. direction)
β relative flow angle (from tangential direction, opposite to $\vec{U}_2$)
Δx horizontal pitch of PIV mesh
Δy vertical pitch of PIV mesh
δ^* displacement thickness
ε_g geometric deflection: $\varepsilon_g = \alpha_{4g} - \alpha^*$
ε_f flow deflection: $\varepsilon_f = \alpha_{4f} - \alpha_{2f}$
φ impeller phase angle
ϕ flow coefficient based on outlet diameter
θ angular coordinate [deg]
θ^* momentum thickness
σ solidity (chord/span)
ψ head coefficient
ω time averaged vorticity on the blade to blade plane

Subscripts:
2 impeller discharge diameter
3 diffuser vane LE diameter
4 diffuser vane TE diameter
5 pump discharge flange
f flow
g geometric
LE leading edge
n generic phase angle
t volute throat
TE trailing edge

INTRODUCTION

In the last years many experimental works, carried out by particle image velocimetry (PIV) or fast response pressure transducers, can be found in literature on centrifugal pumps equipped with vaned diffusers. All these works are however addressed to the flow field unsteadiness related to rotor-stator interaction and/or impeller and diffuser stall (Dupont et al., 2005; Benra et al., 2008; Feng et al., 2009). To the authors' knowledge, the only publication reporting performances of centrifugal pumps with several vaned diffusers is by Arndt et al. (1990). In order to find papers dealing with different radial diffuser performances, literature on centrifugal compressors must be considered. However it should be noticed that, in centrifugal compressors, low solidity vaned diffusers are often preferred to conventional vaned diffuser in order to prevent flow chocking at high flow rates. The well-recognized work by Engeda (2001) compares performances of eight different low solidity diffusers (σ = 0.6 - 0.9) with two vaneless and a conventional diffuser (σ = 1.15). Siva Reddy et al. (2004) investigated the effect of the setting angle of a low solidity vaned diffuser on the performances of a centrifugal compressor; they varied the setting angle of an un-cambered aerofoil from 16° to 32°, step 4°, and found the best efficiency flow coefficient decreasing together with the setting angle. Their static pressure measurements on the blade surface show a very poor static pressure recovery coefficient on the vane PS for almost all the setting angles.

The aim of present paper is the analysis of the time averaged flow field inside diffuser passages for different vane angle settings. Analysis of unsteady phenomena, like impeller blade passage and related phenomena, are beyond the scope of the present paper.

EXPERIMENTAL SET-UP

Test rig

A commercial shrouded impeller (Tab. 1) was fitted in a volute with a vaned diffuser, both made of acrylic, providing an unobstructed optical access of the whole flow field from the impeller discharge to the volute one. Diffuser geometry was obtained from conformal mapping of a linear cascade based on NACA2409 profiles with a stagger angle of 18.7°. The resulting diffuser (Figs. 1, 2) had a vane LE mean line angle α^*=14°. This angle could be adjusted between 10° and 18°. Details about the diffuser are shown in Tab. 2 together with the geometrical data of the diffuser C.A. (circular arc profiles) used in a previous experimental research (Boccazzi et al., 2009). Design criteria for diffuser C.A. (Sedille, 1967) are different from those of the three others; the main feature of this design criteria is the profile of the SS surface, upstream of the diffuser throat, that follows the free vortex streamline at $\alpha = \alpha_2 = 14°$, which represents the foreseen impeller discharge angle at ϕ_{BEP}.

Impeller	
Inlet diameter: D_1 [m]	0.154
Outlet diameter: D_2 [m]	0.224
Discharge blade span: b_2 [m]	0.0413
Discharge blade angle: β_2	29°
Discharge rake angle	12°
Number of blades: N_b	6
Volute	
Constant span: b_t [m]	0.1384

Tab. 1. Impeller and volute geometric data

In order to allow frequent volute and diffuser cleaning, the impeller shaft supports and seals were mounted on linear bearings together with the electric motor and the torque meter. This

Diffuser	Chord [m]	Vane span [m]	N. of vanes	α^*	D_3 (LE) [m]	D_4 (TE) [m]	σ (LE)	D_3/D_2	D_t/D_4
D1	0.1484	0.044	7	10°	0.2485	0.3354	1.33	1.11	1.16
D2	0.1484	0.044	7	14°	0.2458	0.3489	1.35	1.10	1.11
D3	0.1484	0.044	7	18°	0.2432	0.3620	1.36	1.09	1.07
C.A.	0.1833	0.044	7	17.5°	0.2343	0.3600	1.74	1.05	1.08

Tab. 2. Diffuser geometric data

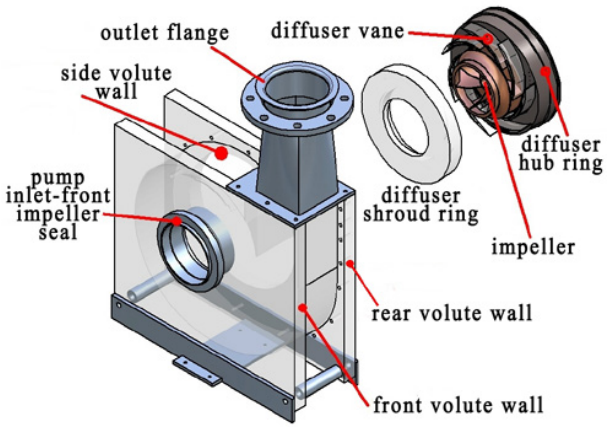

Fig. 1. Expanded view of the pump.

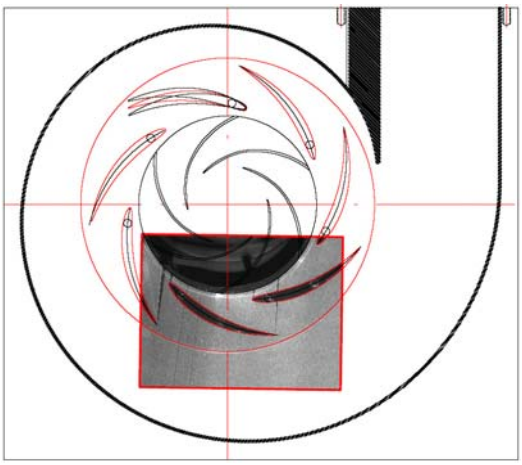

Fig. 2. CCD field of view for diffuser D2. For one of the vanes, the different settings are shown.

configuration and the high transparent casing warping imposed a quite large radial gap in the front impeller seal with a consequent high leakage flow.

Measurement technique

Performance curves were obtained in a closed loop by means of a magnetic flow-meter (uncertainty of ±0.5% of the reading), a differential pressure transducer (700 mbar F.S., ±0.23% of F.S. uncertainty) and an inductive torque meter (50 Nm F.S., 0.5% of F.S. uncertainty). Differential pressure transducers and torque meter were calibrated in the range of interest. Tests were carried out at 600 rpm.

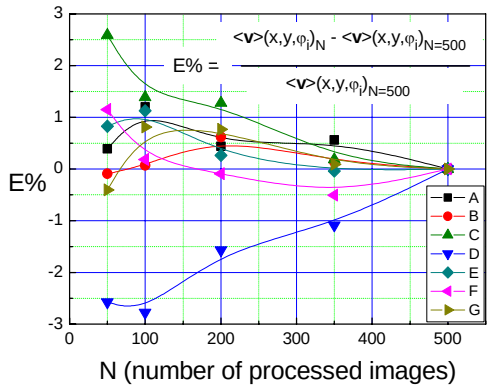

Fig. 3. Percentage error for different numbers of processed images. Every curve corresponds to a point in Fig. 4.

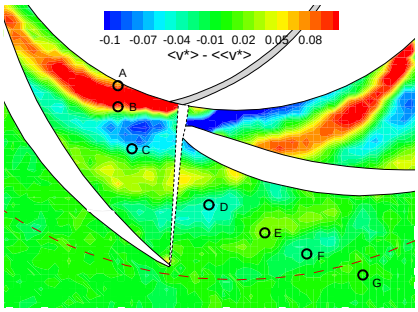

Fig. 4. Positions of the points where percentage errors E% of Fig. 3 were computed.

The 2D-PIV system used in this investigation was composed of a pulsed Nd:YAG laser (532 nm, 200 mJ), a CCD camera (1344x1024 pixels, maximum double frame rate: 5 Hz) and synchronization and frame grabber boards. The phase locked image acquisition was made possible by a magnetic pick-up, faced to the impeller shaft and connected to the synchronization board. Fig. 2 shows the position and width of the field of view where the velocity maps were sampled.

Several tests allowed the choice for the best seeding particles (10 μm diameter silver coated hollow glass micro spheres) and the number of double frame images to be taken for the optimization of the PIV acquisitions. Assuming that 500 double frame images gave reliable phase averaged flow field, a percentage error E% lower than 2% was obtained processing more than 200 double frame images (Fig. 3, 4). PIV processing was carried out by a commercial code. After having recorded 300 double frame images, it was computed the mean pixel value that was subtracted to every image in order to minimize reflections from the impeller blades. An equalization algorithm was then applied in order to enhance double frame images before computing an adaptive cross correlation over an initial correlation

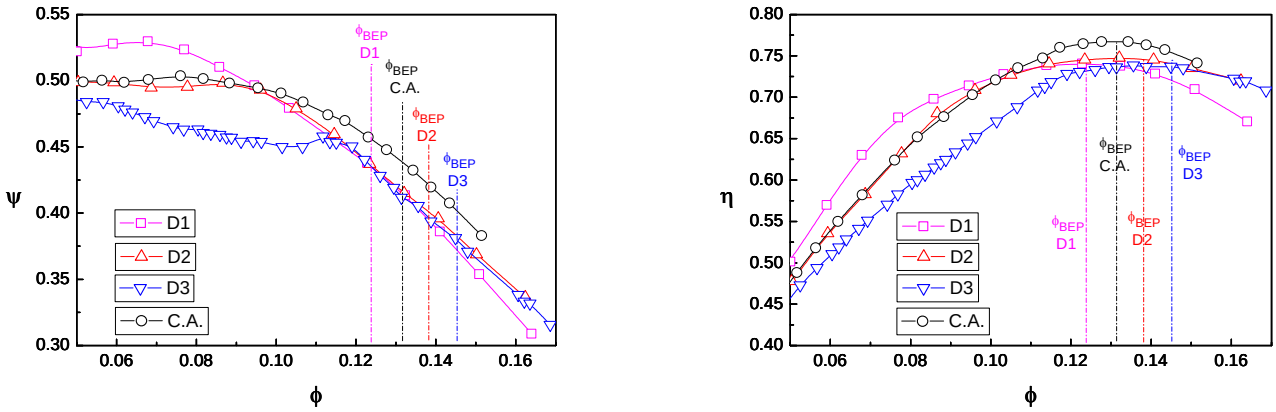

Fig. 5. Pump performance curves.

area of 128×128 pixel with two refinement steps to get a final 32×32 pixel interrogation area with 50% overlap; the resulting sampling mesh was 83x63 cells with a spatial resolution of about 3×10^{-3} m over a diffuser vane throat width of 34.6×10^{-3} m (diffuser D2). The velocity distribution was peak validated with a coefficient equal to 1.2, and range validated assuming the velocity modulus to be bounded between zero and the impeller peripheral speed.

Pump performance curves

The pump performance curves for the different vaned diffusers are shown in Fig. 5. The largest ϕ_{BEP} was obtained using diffuser D3 whereas a higher head rise, at reduced flow coefficients, was obtained using diffuser D1. Diffusers D2 and C.A. showed similar performance curves at reduced flow coefficients ($\phi < 0.11$) but the latter had higher efficiency and head, around BEP, probably related to its lower blockage effect. The best efficiency point and the performance curve, at reduced flow coefficients, seem to be strongly affected by the incidence angle at diffuser vane LE. The pump operates quite well at low capacities, when equipped with diffuser D1; on the contrary, if the diffuser D3 is installed, the pump does not admit a flow coefficient decrease higher than the 20%, from the best efficiency point, without a significant efficiency decrease and change in the characteristic curve slope.

The overall low efficiency values mainly depend on the low volumetric efficiency caused by the large radial gap (10^{-3} m) in the front impeller seal, due to the uneasy alignment of the sliding impeller shaft supports with the transparent pump casing. The consequent high leakage flow should also cause a pre-rotation at impeller inlet affecting pump performance curve slope at low flow coefficients.

MID SPAN DIFFUSER FLOW FIELDS AT BEP

Time averaged flow field

For every rotor phase angle φ chosen between 0° and 60° (impeller blade pitch) with a 5° step, 300 instantaneous flow fields (m) were acquired and averaged in the area of Fig. 2. Averaging the 12 succeeding phase-averaged flow fields, i.e. an impeller blade passage, the time averaged flow field is obtained:

$$\left\langle \vec{v}^{\,*} \right\rangle (x,y)_{\varphi=\varphi_n} = \frac{1}{300}\sum_{m=1}^{300} \vec{v}^{\,*}(x,y,m)_{\varphi=\varphi_n} \qquad \text{phase averaged velocity} \qquad (1)$$

$$\left\langle\left\langle \vec{v}^{\,*} \right\rangle\right\rangle (x,y) = \frac{1}{12}\sum_{n=1}^{12} \left\langle \vec{v}^{\,*} \right\rangle (x,y)_{\varphi=\varphi_n} \qquad \text{time averaged velocity} \qquad (2)$$

The time averaged flow field hides the blade passage effects, i.e. impeller blade wakes and the related unsteadiness, but preserves steady phenomena like the diffuser vane LE blockage effect and volute geometry effect.

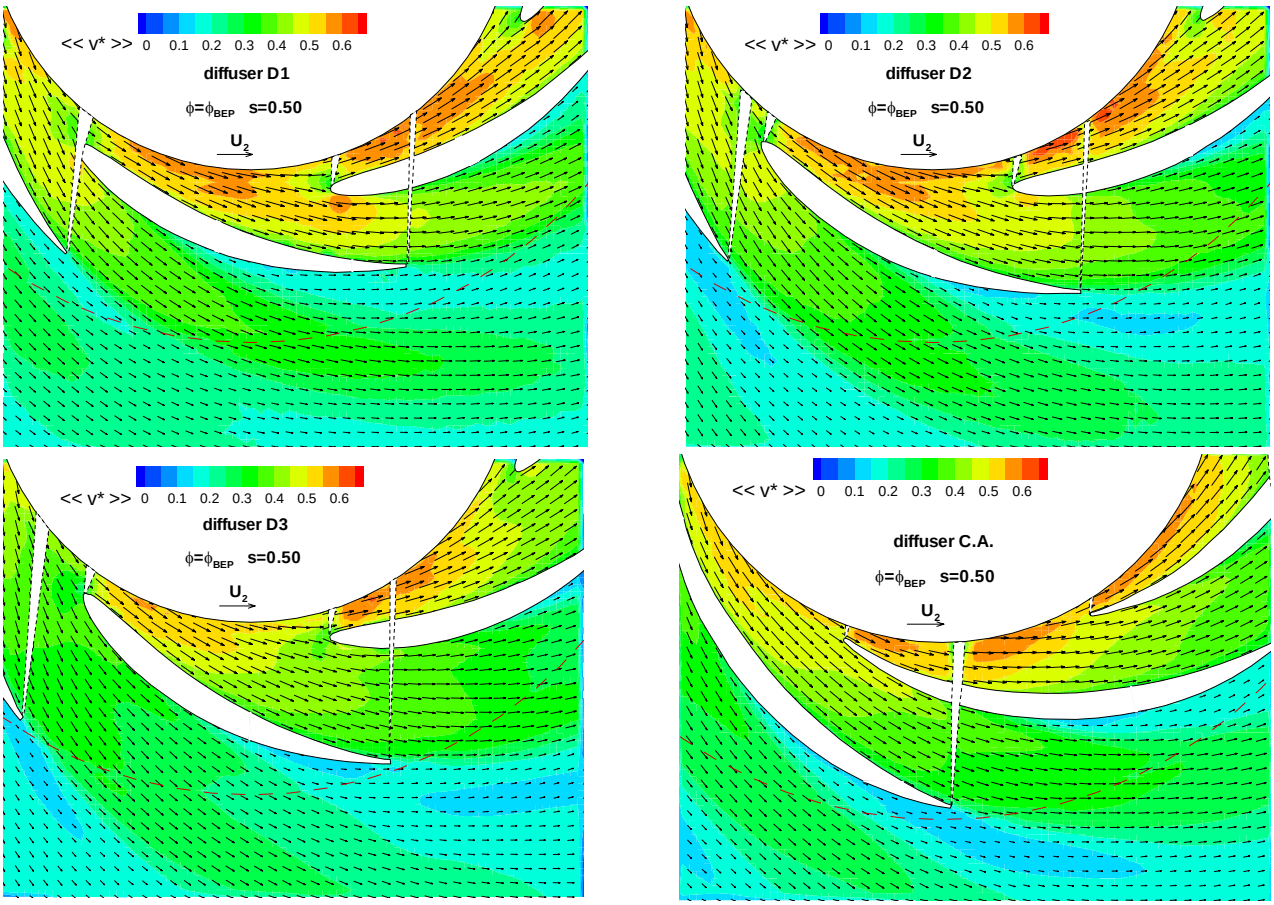

Fig. 6. Time averaged flow fields for different diffusers at $\phi = \phi_{BEP}$. Only alternate vectors are shown for clarity.

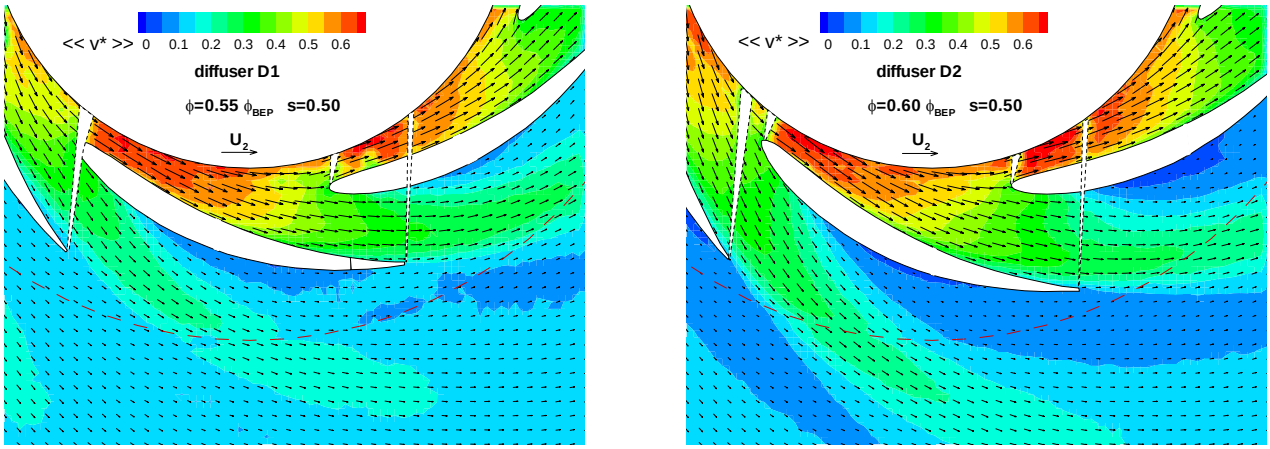

Fig. 7. Time averaged flow fields for diffuser D1 and D2 at reduced flow coefficients.

Time averaged flow fields, for different diffusers, are plotted in Fig. 6. The white strips show the vane LE and TE shadows affecting measuring reliability over the evidenced areas. The red dashed arc shows the outer diameter of the diffuser vane support disk where a sudden cross section increase occurs (Volute/Vane span = 3.15).

The following considerations can be pointed out:

- Different velocity distributions, among different diffuser passages, are probably to be ascribed to the volute geometry that is not optimized for the exit angle of the different diffusers even at their BEP. This feature inevitably affects the discussion of the experimental results and it will be discussed whenever it will occur.

- Blockage effect of the diffuser vane LE modifies the impeller outlet flow field. Due to its lower blockage, a lower effect is produced by the diffuser C.A.
- A velocity peak, at the PS of the diffuser vane LE is evident in diffuser D1, decreases in diffuser D2 and vanishes in diffuser D3 and C.A. This velocity peak, expected on the SS in linear cascades, seems to be related to the flow acceleration in the narrow diffuser throat of diffuser D1.
- A boundary layer thickness growth is noticeable on the convex side (PS) of the diffuser vanes. This boundary layer thickness is not affected by the impeller blade passage: phase averaged velocity maps, not reported in this paper, do not show appreciable influence of the impeller blade passages on this flow feature.

Similar boundary layer thickness growths are also reported in other radial diffusers by M. Sinha et al. (2000), Ziegler et al. (2003) and F. Benra (2008).

Even at reduced flow coefficient (Fig. 7) no separation or boundary layer thickness growth is observed on the vane SS whereas a large separation, increasing with α^*, is evident on the vane PS.

In order to get more insights into the PS boundary layer thickness growth at ϕ_{BEP}, the time averaged vorticity:

$$\omega = \frac{\langle\langle v\rangle\rangle(i+1,j)-\langle\langle v\rangle\rangle(i-1,j)}{2\Delta x} - \frac{\langle\langle u\rangle\rangle(i,j+1)-\langle\langle u\rangle\rangle(i,j-1)}{2\Delta y} \qquad \text{time averaged vorticity} \qquad (3)$$

was computed and the resulting maps are plotted in Fig. 8 for the different diffusers together with stream traces.

The maximum negative vorticity is consistent with the presence of the vane SS boundary layer whereas the maximum positive vorticity is located on the boundary of the almost uniform flow that can be regarded as the free stream flow. It should however be noticed that the free stream flow is affected by the vorticity of the impeller flow field. In author's opinion vorticity maps enlighten

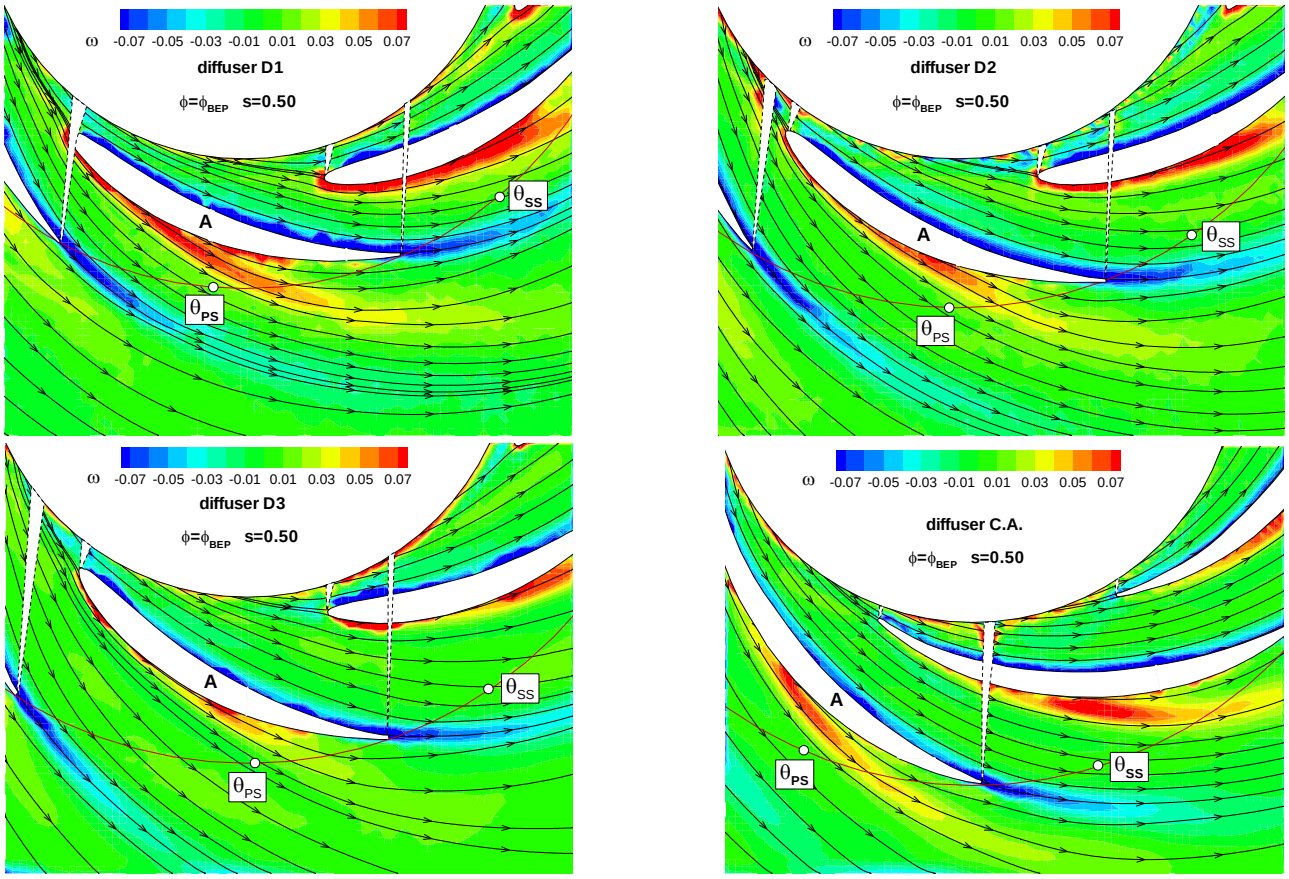

Fig. 8. Time averaged vorticity and stream traces for different diffusers at ϕ_{BEP}. White dots show the free stream boundaries that were used to compute δ* and θ* [4, 5, 6, 7].

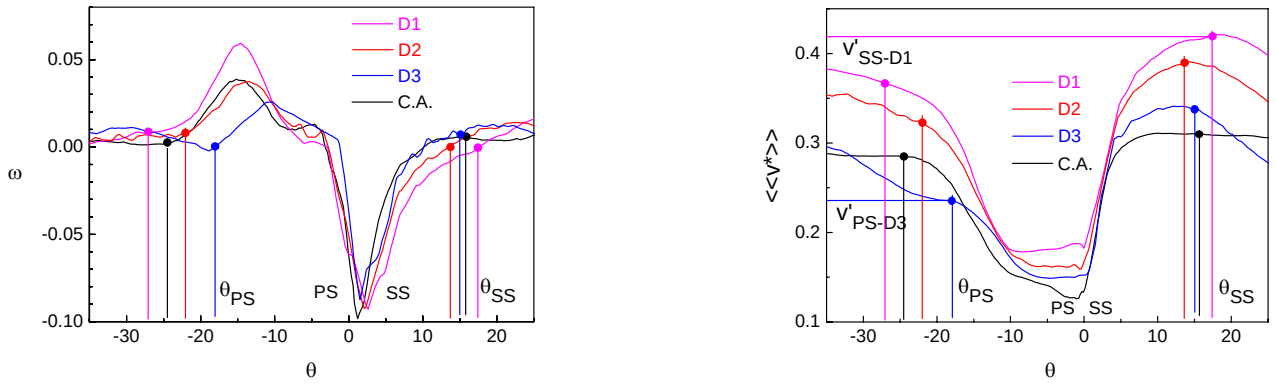

Fig. 9. Time averaged vorticity (a) and non dimensional time averaged velocity (b) at the vaned diffuser discharge (θ=0 at vane TE). Different vertical lines and coloured dots show θ_{PS}, θ_{SS} and the related velocities (v') used for computing displacement and momentum thickness.

boundary layer borders with vorticity layers diverging from the diffuser vane PS. The velocity and vorticity values were extracted (interpolation step Δθ) along the diffuser vane TE circumference (D_4), around the blade labeled as A, and the results are plotted in Fig. 9. These plots have been used in order to determine the limits of integration to compute the boundary layer parameters (Japikse, 1996):

$$\delta^*_{SS} = \cos(\alpha_{4g} - \alpha_{3g})\Delta\theta \frac{\pi D_4}{360} \sum_{0}^{\theta_{SS}} \left(1 - \frac{\langle\langle v^* \rangle\rangle(\theta)}{v'_{SS}}\right) \qquad \text{SS displacement thickness} \qquad (4)$$

$$\delta^*_{PS} = \cos(\alpha_{4g} - \alpha_{3g})\Delta\theta \frac{\pi D_4}{360} \sum_{\theta_{PS}}^{0} \left(1 - \frac{\langle\langle v^* \rangle\rangle(\theta)}{v'_{PS}}\right) \qquad \text{PS displacement thickness} \qquad (5)$$

$$\theta^*_{SS} = \cos(\alpha_{4g} - \alpha_{3g})\Delta\theta \frac{\pi D_4}{360} \sum_{0}^{\theta_{SS}} \left(\left(1 - \frac{\langle\langle v^* \rangle\rangle(\theta)}{v'_{SS}}\right)\frac{\langle\langle v^* \rangle\rangle(\theta)}{v'_{SS}}\right) \qquad \text{SS momentum thickness} \qquad (6)$$

$$\theta^*_{PS} = \cos(\alpha_{4g} - \alpha_{3g})\Delta\theta \frac{\pi D_4}{360} \sum_{\theta_{PS}}^{0} \left(\left(1 - \frac{\langle\langle v^* \rangle\rangle(\theta)}{v'_{PS}}\right)\frac{\langle\langle v^* \rangle\rangle(\theta)}{v'_{PS}}\right) \qquad \text{PS momentum thickness} \qquad (7)$$

where $\cos(\alpha_{4g} - \alpha_{3g})$ takes into account the flow deflection and θ_{SS} and θ_{PS} (Fig. 9a) correspond respectively to the boundaries of the negative and positive vorticity layers; the related time averaged velocities, v'_{SS} and v'_{PS} at diameter D_4 (Fig. 9b), were assumed as the free stream velocities. The choice of separately computing SS and PS displacement and momentum thicknesses at the vane TE is somehow questionable but it is in author's opinion that it could be useful in order to analyze the flow features of different diffusers.

Computed displacement and momentum thicknesses are plotted in Fig. 10 for different diffusers. It must be noticed at first that they are affected by the uneven flow distribution of the different diffuser passages. However, both Reynolds number and flow rate effects (such as incidence at the vane LE and blade loading) are expected to slightly affect the boundary layer thickness when a 10% velocity difference between adjacent diffuser passages occurs.

Suction side displacement and momentum thicknesses are lower than the ones on the pressure side and they slightly decrease if the diffuser vane LE mean line angle (α^*) increases. Pressure side displacement thickness, on the contrary, shows a remarkable decrease for diffuser D3 ($\alpha^* = 18$) although not so evident in the maps of Fig. 6. Suction side displacement and momentum thicknesses for diffuser C.A. (solid symbols in Fig. 10 and followings) are slightly lower than the ones of the other diffusers: this is consistent with the free vortex shape of the suction side surface upstream of the diffuser throat (Sedille, 1967); on the contrary, the high values of the pressure side

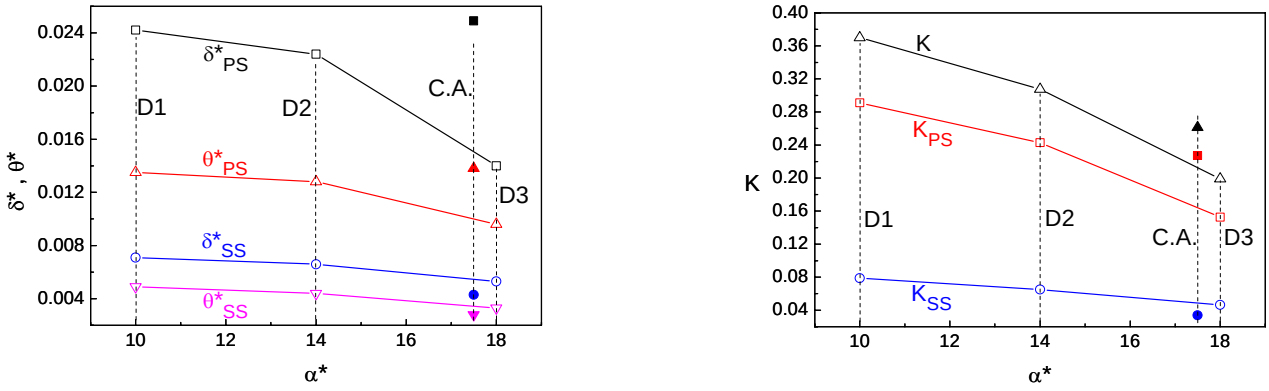

a) **b)**

Fig. 10. Displacement and momentum thicknesses (a) and total pressure loss coefficients (b) for the different diffusers; solid symbols refer to diffuser C.A.

boundary layer parameters are probably due to the high curvature of the pressure side at the diffuser discharge.

The values of displacement and momentum thickness allowed to compute the total pressure loss coefficient K from the following expression proposed by Japikse (1996) for radial diffusers and derived, for linear cascades, by Lieblein and Roudebush (1956):

$$K = 2\left(\frac{\theta^*}{c}\right)\frac{\sigma_{TE}}{\cos\alpha_{4g}}\left(\frac{\cos\alpha_{3g}}{\cos\alpha_{4g}}\right)^2\left[1-\frac{\theta^*}{c}\frac{H\sigma_{TE}}{\cos\alpha_{4g}}\right]^{-3}\frac{2H}{3H-1} \qquad \text{total pressure loss coefficient} \qquad (8)$$

where $H = \delta^*_{SS}/\theta^*_{SS}$ for K_{SS} and $H = \delta^*_{PS}/\theta^*_{PS}$ for K_{PS}: also for this coefficient it was preferred to separate suction side from pressure side profile losses. The solidity σ_{TE} is computed at the vane TE although Japikse does not specify where to compute it.

Loss coefficient K (Fig. 10b) is only a rough estimation of the diffusion losses as it does not take into account the pressure gradient due to the centrifugal field and also the significant secondary flows occurring in the diffuser passages (discussed later on). The total pressure loss coefficient can however be useful for the comparison of the four different diffusers with similar centrifugal fields.

To get more insights into the time averaged flow fields of the different diffusers, the pitch averaged flow angles at diffuser inlet and outlet are computed: 200 interpolated values of «u» and «v» components have been extracted from the time averaged maps along D_2 (actually 1.013 D_2) and D_4 diameter circumferences. From the x and y coordinates of the impeller axis, obtained by superposition of the PIV images on the CAD design (Fig. 2), the time averaged radial velocity component was computed together with the absolute and relative time averaged angles, respectively «α_2»(i, D_2) and «β_2»(i, D_2). Similarly the «α_4»(i, D_4) angle at D_4 diameter circumference was obtained. The pitch mass averaged angles have then been computed:

$$\alpha_{2f} = \frac{\sum_{i=1}^{200}\langle\langle\alpha_2\rangle\rangle(i,D_2)\langle\langle v_{r2}\rangle\rangle(i,D_2)}{\sum_{i=1}^{200}\langle\langle v_{r2}\rangle\rangle(i,D_2)} \qquad \text{pitch averaged absolute flow angle at impeller discharge} \qquad (9)$$

$$\beta_{2f} = \frac{\sum_{i=1}^{200}\langle\langle\beta_2\rangle\rangle(i,D_2)\langle\langle v_{r2}\rangle\rangle(i,D_2)}{\sum_{i=1}^{200}\langle\langle v_{r2}\rangle\rangle(i,D_2)} \qquad \text{pitch averaged relative flow angle at impeller discharge} \qquad (10)$$

$$\alpha_{4f} = \frac{\sum_{i=1}^{200}\langle\langle\alpha_4\rangle\rangle(i,D_4)\langle\langle v_4\rangle\rangle(i,D_4)}{\sum_{i=1}^{200}\langle\langle v_4\rangle\rangle(i,D_4)} \qquad \text{pitch averaged absolute flow angle at diffuser discharge} \qquad (11)$$

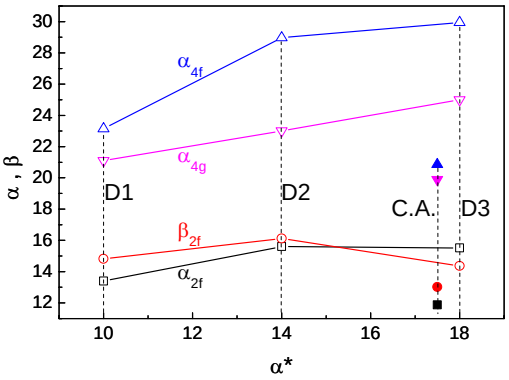

Fig. 11. Flow and geometrical angles for the different diffusers (solid symbols for diffuser C.A.).

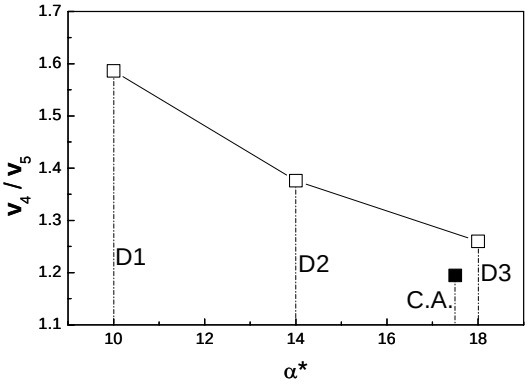

Fig. 12. Velocity ratio between diffuser and volute discharge (v_4 is the mass averaged velocity at the TE of the diffuser discharge).

These angles are plotted in Fig. 11 for different diffusers (different α*). The reliability of such computation is affected by the different velocity distribution between different diffuser passages. However the diffuser vanes of diffusers D1, D2 and D3 have similar angular gaps from the volute throat and comparable flow angles are therefore expected for these diffusers.

DISCUSSION OF THE EXPERIMENTAL RESULTS

In spite of the low spatial resolution of the PIV measurements, a PS boundary layer thickness growth (Figs. 6 and 8), unexpected on the diffuser vane PS for annular diffusers, have been evidenced at ϕ_{BEP}. Total pressure loss coefficient K (8) is mainly affected by this boundary layer thickness growth (Fig. 10b). The displacement and momentum thicknesses (Fig. 10a), decreasing with the α^* increase, lead to a total pressure loss decrease (Fig. 10b).

Diffuser D1 (α^*=10°) has a poor kinetic energy recovery (Fig. 6) that is related to its high displacement thickness (Fig. 10a), so a further velocity decrease occurs in the volute (Fig. 12). On the other hand, the low setting angle of diffuser D1 implies acceptable incidence angles at reduced flow coefficients. Fig. 5 shows, in fact, a wide range of flow coefficient with high efficiency values. Moreover, diffuser D1 exhibits a regular slope of the performance curve down to 50% of ϕ_{BEP} (Fig. 5) providing a stable operating behavior.

Diffuser D3 (α^*=18) allows a more regular recovery of the inlet kinetic energy (Figs. 6, 12) at ϕ_{BEP} but any incidence angle increase ($\alpha^* - \alpha_{2f} \sim 2.5°$ in Fig. 11) negatively affects pump performances: performance curve (Fig. 5) indeed shows positive slope between 0.6 and 0.8 of ϕ_{BEP}; moreover a small flow coefficient reduction, from the BEP one, implies a larger efficiency decrease than that of the other diffusers.

Impeller slip (Fig. 11) is weakly affected by the diffuser setting angle (α^*) as time averaged relative angles β_{2f} range from 14.8°, for diffuser D1, to 16°, for diffuser D2, and to 14.4°, for diffuser D3. An increase of the incidence angle, from -3.4° (D1) to -1.6° (D2) and to 2.5° (D3), was consistently measured. Lower values of β_{2f} (13°) and higher values of the incidence angle (5.7°) were measured for diffuser C.A.

For all the diffusers, except for D1 (α^* = 10°), a sort of over-turning is measured as reported in Fig. 11, where $\alpha_{4f} > \alpha_{4g}$, and in Fig. 13 where geometric and flow deflections are plotted. The over-turning ($\varepsilon_f > \varepsilon_g$) is usually related to secondary flows that cannot be evidenced by 2D-PIV. Measurements at different blade span were taken for diffuser D2; they show an uneven flow distribution in different span wise planes (Fig. 15) giving the profile of the discharge flow angle plotted in Fig. 14 where a strong under-turning at the hub suggests the occurrence of significant secondary flows. It must be noticed that noteworthy impeller secondary flows are very common in high specific speed pumps where impeller boundary layer thickness is always significantly wider at

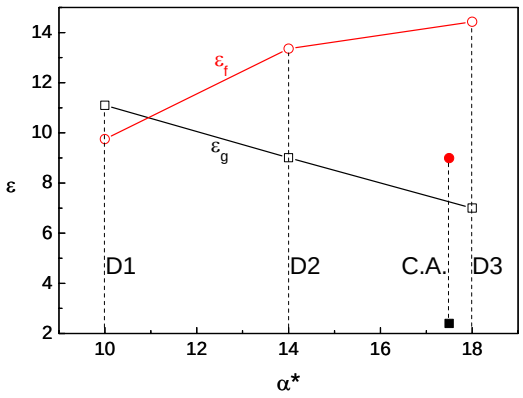

Fig. 13. Flow and geometrical deflections for the different diffusers (solid symbols for diffuser C.A.).

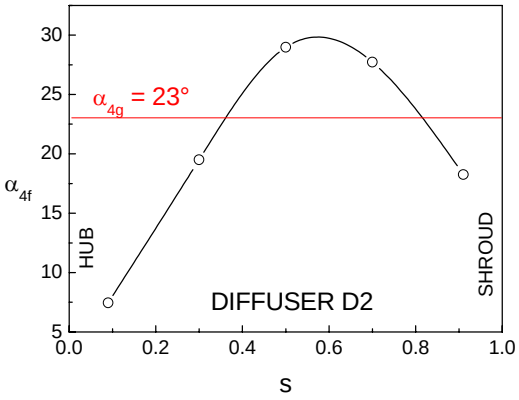

Fig. 14. Discharge flow angle at different diffuser spans for diffuser D2.

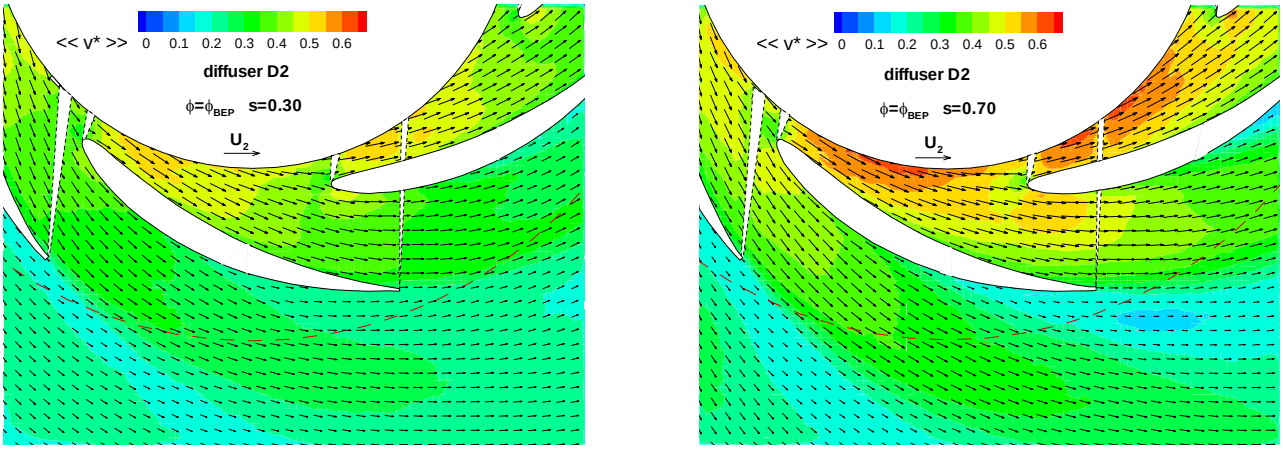

Fig. 15. Time averaged flow fields for diffuser D2 at two different spans: s = 0.3 and s = 0.7. The map at s = 0.5 is in Fig. 6.

the hub than at the shroud. This over-turning seems not however related to the PS boundary layer thickness growth: in fact, for diffuser D1 with the maximum boundary layer displacement thickness (Fig. 10), no over-turning ($\varepsilon_f = 9.8°$, $\varepsilon_g \cong 11°$) can be noticed.

CONCLUSIONS

The diffuser vane setting angle slightly affects the impeller slip; conversely it fairly modifies the BEP flow coefficient being the latter a trade-off between the optimum operating conditions of the impeller and the ones of the diffuser when operated separately. A low setting angle improves pump performances at reduced flow coefficients. Conversely a high setting angle improves pump performances at high flow coefficients but dramatically reduces pump performances at the lower ones. It should however be noticed that the change of BEP flow coefficient is not only a matter of diffuser incidence: in fact, whereas a setting angle (α^*) increase, from 10° (diffuser D1) to 14° (diffuser D2), affects the diffuser inlet flow field with an increase of the flow angle (α_{2f}) from 13.4° to 15.6°, the same setting angle increase, from 14° (diffuser D2) to 18° (diffuser D3) does not significantly affect the inlet flow field with a consistent incidence angle increase

A rounded diffuser vane LE does not improve pump performances at reduced flow coefficients as no significant separation ever occurs on the vane SS.

An over-turning has been evidenced at mid-span for diffusers D2 and D3. Measurements at different spans, for diffuser D2 evidenced an under-turning near the walls, particularly at the hub. This flow feature suggests the occurrence of secondary flows, at diffuser discharge, that could be

determined as the ones of the impeller, which are typically considerable in high specific speed pumps.

Diffuser design criteria based on conformal mapping of linear cascades seem to be quite unprofitable as the resulting radial flow field has completely different features from the ones of the axial flow field. In fact, conformal scaling to radial diffuser does not preserve the solidity, changing between inlet and outlet, the vane curvatures and the shape of the semi-vaned space, leaving a wider semi-vaned region at the TE; in this region the wall is represented only by the PS of the vane which is not balanced by an opposite wall. In radial diffusers, separation is most likely to occur on vane PS whereas in axial diffusers, with positive incidence angles, it always occurs on the vane SS.

REFERENCES

N. Arndt, A.J. Acosta, C.E. Brennen and T.K. Caughey, 1990. "Experimental Investigation of Rotor-Stator Interaction in a Centrifugal Pump With Several Vaned Diffusers". *Journal of Turbomachinery* Vol. 112, January.

A. Boccazzi, R. Miorini, R. Sala and F. Marinoni, 2009, "Unsteady Flow Field in a Radial Pump Vaned Diffuser". In: 8th European Turbomachinery Conference, Graz-Austria.

F.K. Benra, J. Feng, H.J. Dohmen, 2008, "PIV Measurements of Unsteady Flow in a Diffuser Pump at Different Flow Rates", Proc. ISROMAC 12-2008-20024.

P. Dupont, G. Caignaert, G. Bois, T. Schneider, 2005, "Rotor-Stator Interactions in a Vaned Diffuser Radial Flow Pump", Proc. ASME FEDSM2005-77038.

A. Engeda, 2001. "The design and performance results of simple flat plate low solidity vaned diffusers". Proc. Instn Mech Engrs, Vol. 215 Part A.

J. Feng, F-K. Benra and H.J. Dohmen, 2009. "Time-Resolved Particle Image Velocimetry (PIV) Measurements in a Radial Diffuser Pump". ASME FEDSM2009-78297.

D. Japikse, 1996, *Centrifugal Compressor Design and Performance*. Concepts ETI, Inc.

S. Lieblein and W.H. Roudebush, 1956, "Theoretical loss relations for low-speed two-dimensional-cascade flow". *NACA TN* 3662.

M. Sedille, 1967. "*Turbo-Machines Hydrauliques et Thermiques*". Masson et Cie Editeurs, Paris.

M. Sinha and J. Katz, 2000, "Quantitative Visualization of the Flow in a Centrifugal Pump With Diffuser Vanes-I: On Flow Structures and Turbulence", *JFE*, vol. 122, pp. 97-107.

T.Ch. Siva Reddy, G.V. Ramana Murty, P. Mukkavilli and D.N. Reddy, 2004. "Effect of the setting angle of a low-solidity vaned diffuser on the performance of a centrifugal compressor stage". Proc. Instn Mech Engrs, Vol. 218 Part A.

K.U. Ziegler, H.E. Gallus and R. Niehuis, 2003. "A Study on Impeller-Diffuser Interaction – Part I: Influence on the Performance". *Journal of Turbomachinery* Vol. 125, January.